



Ultra-long (290 km) remote interrogation sensor network based on a random distributed feedback fiber laser

V. DEMIGUEL-SOTO,* D. LEANDRO, AND M. LOPEZ-AMO

Universidad Pública de Navarra, Dept. of Electrical and Electronic Engineering and ISC, Campus de Arrosadia, 31006, Pamplona, Spain

*veronica.demiguel@unavarra.es

Abstract: In this work, an interferometric sensor has been interrogated 290 km away from the monitoring station, reaching the longest distance in fiber optic sensing up to date. This has been attained by employing a double-pumped random distributed feedback fiber laser as the light source for a fiber optic low-coherence interferometry scheme. Additionally, the capability of the system to achieve coherence multiplexing for ultra-long range measurements (up to 270 km) has been proved, without presenting crosstalk between the sensors. The use of coherence multiplexing together with a random distributed feedback fiber laser addresses two of the main limitations of long-range sensing setups: their limited multiplexing capability and the need to reach the maximum monitoring distance.

© 2018 Optical Society of America under the terms of the [OSA Open Access Publishing Agreement](#)

1. Introduction

Optical fiber systems for remote sensing have attracted a lot of interest during the last years due to their ability to monitor a large range of parameters at long distances, without requiring power supply at the sensor location. Some of these applications include the detection and propagation of tsunamis, which is of vital importance for the protection of natural environment, coastal population and structures [1]. Monitoring strain changes at volcanic areas can predict the possible evolution towards critical situations [2]. In addition, health monitoring of offshore platforms allows reducing costs, improving safety and increasing their operational lifetime [3]. Remote systems must face different challenges, but two of them are especially significant: to enlarge the distance between the sensor and the monitoring station and to multiplex several sensors on a single network.

Lately, several schemes for remote sensing have been proposed [4] using different types of amplification. In [5], a sensor located 230 km away from the monitoring station was interrogated using a high-speed sweep-wavelength light source amplified by an Erbium-doped fiber amplifier. Raman amplification was employed in [6] to achieve a maximum distance of 250 km multiplexing four fiber Bragg grating (FBG) sensors. Finally, an optical time domain reflectometer monitored a long-period grating displacement sensor at 253 km, reaching the maximum distance up to date [7].

The main purpose of multiplexing fiber optic sensors is to reduce the total cost of the system by sharing a number of devices of the network. Several multiplexing techniques have been investigated, offering specific benefits for each particular application [8,9]. In the same manner, hybrid methods of modulation formats within the same network have been considered [10,11]. Among all the multiplexing approaches, coherence multiplexing (CM) uses light sources with low coherence length on interferometric setups to multiplex several sensors into a single optical signal [12]. CM avoids the relatively complex requirements of time [13] or wavelength-division multiplexing [14], such as synchronization and frequency ramping of the optical source, respectively. However, in CM the geometry of each sensor must be carefully designed so the optical path differences (OPD) of each sensing interferometer are in different ranges. Then every sensing signal can be de-multiplexed by selecting its OPD in the local receiving

interferometer. Coherence-multiplexed systems have been widely used in fiber-optic sensing, multiplexing up to 10 sensors in [15] and measuring physical parameters such as temperature, displacement and strain [16–18].

Commonly, CM is employed in sensor systems based on fiber optic low-coherence interferometry (FOLCI) [19,20]. Temperature [21], pressure [22], strain [23] and refractive index [24] are some parameters that can be measured with high accuracy using this approach. Although FOLCI technique is intensity-based, the measurement accuracy is ideally insensitive to optical power fluctuations between the monitoring and the sensor location. Accordingly, higher resolutions are provided if compared to conventional intensity-based sensors. Moreover, FOLCI systems allow to measure absolute displacements, without the requirement of a previous characterization of the sensors. Due to the intrinsic need of short-coherence length in FOLCI, broad-band light sources are generally employed. However, the low output power of broad-band sources (compared to laser sources) causes that low-coherence based systems are generally not well suited for long-range applications.

During the last years, random distributed feedback fiber lasers (RDFB-FL) have been investigated extensively owing to their particularities as light sources when compared to conventional laser systems [25]. Their high power, mode-less behavior, stability and long cavities make them especially convenient for ultra-long range applications [26]. Besides, RDFB-FL can be internally modulated without frequency restrictions, which was used in [10] to monitor ten FBGs at 200 km. In that work, it was employed a hybrid technique which combined wavelength-division with time-domain multiplexing. This approach considerably improved the multiplexing capability of ultra/long networks compared to other remote structures previously proposed. In the present study, the natural coherence length of RDFB-FLs is particularly important since it is short enough to make them suitable for FOLCI.

The feasibility of using RDFB-FL in low-coherence interferometry and coherence-multiplexing is demonstrated. In order to show its potential, two experiments have been carried out. The remote interrogation of an interferometric sensor has been achieved 290 km away from the header. This is, as far as the authors are aware, the longest distance for a remote fiber optic sensing system. In addition, the capability of the technique to achieve coherence multiplexing has been validated by interrogating two sensors at a distance of 270 km. Only one local receiving interferometer has been required to scan the displacement applied to both sensors, without crosstalk. This has been achieved by exploiting the particular properties of RDFB-FL, such as their high power and relatively short coherence length, in combination with a low-coherence interferometry approach. These results show the great potential of FOLCI schemes in remote sensing applications when using RDFB-FL as the light source.

2. Experimental set-up and principle of operation

2.1. Displacement sensor at 290 km

The initial setup (Fig. 1) is formed by three differentiated parts: the laser source, the transmission channel and the sensing interferometer.

A fiber laser requires an optical cavity to confine the light, which is then amplified until reaching the lasing threshold. In this setup, a single-arm distributed cavity is used, where a loop mirror recirculates the backscattered light in the laser cavity. The loop mirror redirects the light through port 2 of a 3-port optical circulator. The distributed mirror is formed by the 50 km + 290 km of standard single mode fiber (Sterlite OH-Lite-E, with an attenuation of 0.19 dB/km), which provides a weak feedback along the fiber because of the Rayleigh scattering effect. This distributed feedback is the principle of generation in RDFB-FL. Two wavelength division multiplexers (WDM) are employed to inject two pump lasers (RLD-5K-1360 and RLD-5K-1445) into the distributed cavity. Then, the fiber acts as the medium for the amplification due to the stimulated Raman scattering effect. Both WDMs are connected in series separated by a 50 km SMF fiber spool. This fiber allows the generation of a secondary pump close to 1445 nm and initiates the generation of a 2nd Stokes line close to 1550 nm. This is latter assisted by

the 1445 nm pump laser. In this manner, the pump laser at 1445 nm combine with the first Stokes wave generated by the pump at 1360 nm. The resulting emission generates and amplifies along the cavity an emission line at 1550 nm. At the end of the cavity, right before the sensing interferometer, an optical isolator is employed to prevent any feedback that could influence the laser performance.

The transmission channel is composed by two identical 290 km optical paths. The first one forms part of the single-arm forward-pumped RDFB-FL, which illuminates the interferometric sensor. The second path guides the signal modulated by the sensor back to the detection system. Both the illuminating signal and the response of the sensors cannot share the same transmission channel because the counter-propagating noise in the arm of the laser is higher than the sensor response. In this manner, two different paths are used in the experiment, doubling the fiber needed in the system. However, a cable of two fibers can be used instead of a single-fiber cable, which does not present a significant increment in the final costs of the installation.

Finally, two Mach Zehnder interferometers (MZI) compose the FOLCI sensing scheme: a sensing interferometer (SI) located 290 km away from the monitoring station and a local receiving interferometer (LRI). Two 50:50 optical couplers (C1, C2 and C3, C4) connected by two SMF arms (L1, L2 and L1', L2') compose each interferometer, respectively. The lengths of each arm in the SI and LRI are: $L1 \approx L1' = 2.16$ m, $L2 = 9.04$ m and $L2' = 9.03$ m. Two separate displacement stages, equally formed by a fixed platform and a mobile micro-positioner (Newport M423), apply displacement in L2 and L2' arms. The detected interference depends on the polarization of the two interfering signals that arrive at the LRI. Therefore, a polarization controller is connected in the LRI arm L1' so the fringe visibility of the interference signal is maximized. Finally, the optical power reaching the monitoring station is measured by an optical multimeter (ANDO AQ-2140) connected at the output of the LRI.

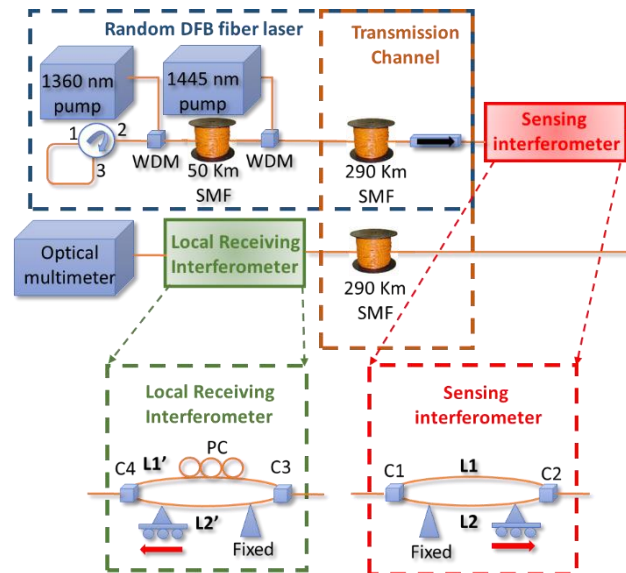


Fig. 1. Set-up 1. Schematic set-up with one sensor.

2.2. Coherence multiplexing of two displacement sensors at 270 km

To evaluate the capability of the system to achieve coherence multiplexing, a second setup is proposed (Fig. 2). This is composed by three MZI: two coherence multiplexed sensing interferometers (SI1 and SI2) located 270 km away from the monitoring station and a LRI. The SIs are arrayed in parallel between the input and output buses by two optical couplers 50:50, CA and CB, following an intrinsic-reference ladder configuration [12]. The arms of CA and

CB present a length of $L_a \approx L_a' \approx L_b \approx L_b' = 1.08$ m. The detection of the sensors is done by the LRI connected in series, which interrogates both SIs in a single displacement sweep. SI1 and the LRI are the same as in set-up 1. The second SI (SI2) is formed by two 50:50 optical couplers (C5 and C6) connected by two SMF arms (L3 and L4), with a length of 2.16 m and 9.05 m, respectively. A polarization controller is used in the LRI arm L1' to maximize the fringe visibility of the interference signal detected.

The light source used in this scheme is the same as in 2.1., where a single sensor is interrogated. However, the transmission channel of the fiber laser is reduced to 270 km due to the larger number of couplers used in this experiment. However, power losses can be modest if the coupling ratios of the couplers used are properly chosen, even if several sensors are multiplexed [27].

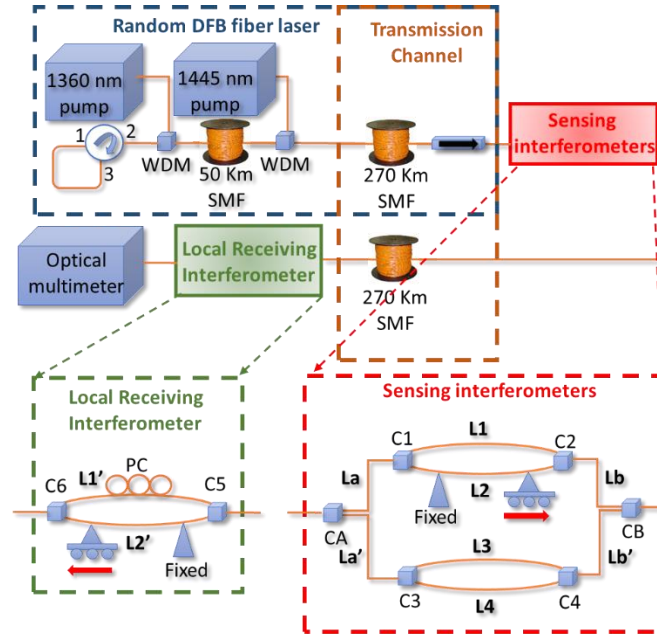


Fig. 2. Set-up 2. Schematic set-up with two sensors.

2.3. Principle of operation

A FOLCI system requires at least two illuminated interferometers sharing optical paths. The OPDs of both interferometers must differ a length several times larger than the coherence length of the light source, L_c . Providing this, no coherent interference will be generated by each interferometer individually. In the case of using MZ interferometers, if the difference between the OPDs of the SI ($OPD_1 = |L_1 - L_2|$) and the LRI ($OPD_r = |L_1' - L_2'|$) is tailored to be shorter than L_c , $|OPD_r - OPD_1| < L_c$, interference will result and the optical intensity detected at the output of the LRI (I) will be given by:

$$I(\Delta L) = I_0 \left(1 + \sqrt{K_1 K_2 K_3 K_4} \exp\left(-\frac{2\Delta L}{L_c}\right) \cos(k\Delta L) \right) \quad (1)$$

where $\Delta L = OPD_r - OPD_1$, k is the wavenumber, I_0 the total optical power arriving at the detector and K_1, K_2, K_3 and K_4 are the power split ratios of the couplers used in the SI and the LRI respectively [20].

In FOLCI structures, low-coherence broadband sources such as light-emitting diodes (LED) are widely employed. As their spectral width varies from 30 to 60 nm, they offer short coherence lengths (compared to laser sources); therefore, narrower interferograms are obtained.

In this work, a RDFB-FL serves as the broadband source needed for a FOLCI system. Although the inherent line-width of RDFB-FL is much narrower than the spectral width of LED sources (several nanometers), it is considerably wider than in traditional laser sources and also presents a high output power (hundreds of milliwatts [25]). This high power combined with a coherence length under the millimeter make RDFB-FLs perfect candidates to allow the use of FOLCI in long-range schemes. In Fig. 3(a), an example of the normalized measured interferogram at the output of the FOLCI system for a single sensor is presented. In order to verify the experimental results, simulations have been performed and presented in Fig. 3(b), showing a good agreement. The simulated interferogram has been obtained through Eq. (1), calculating the values of I for ΔL from -1.2 mm to 1.2 mm, considering a coherence length of 0.808 mm, $k = 2\pi/1550$ nm and $K1 = K2 = K3 = K4 = 0.5$.

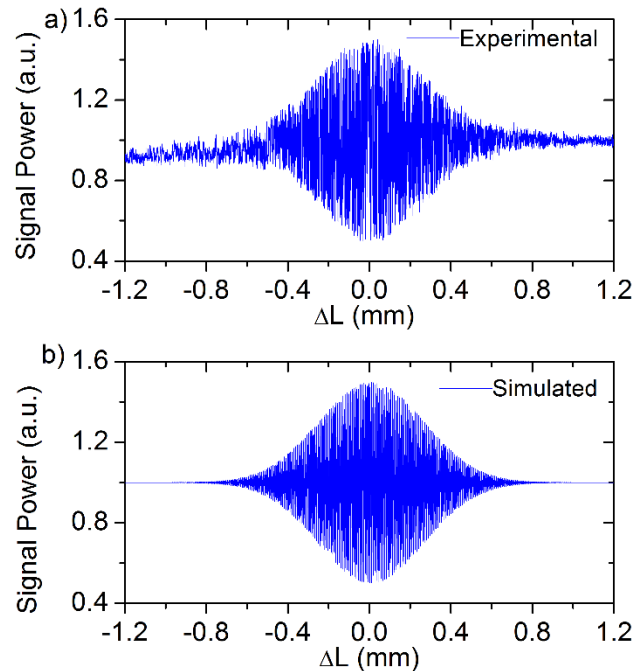


Fig. 3. Normalized a) experimental and b) simulated traces detected at the output of the FOLCI scheme.

According to theory, both traces present a Gaussian profile with a total width $\approx 2Lc$. If any variation is caused in the OPD of the SI (OPD1), the value of ΔL will be modified. As a result, the fringe visibility and the phase of the signal detected at the output of the FOLCI system I will be shifted, altering the position of the central fringe. Thus, absolute changes in OPD1 can be determined by measuring the displacement of the central fringe. To interrogate the sensors, the OPD in the local receiving interferometer (OPDr) is modified using a translation stage and a displacement sweep. In this manner, the power received at the power-meter is detected every step to reconstruct the interferogram. Consequently, the position of the central fringe (i.e. OPD1) can be inferred for every complete sweep.

To avoid signal overlapping when interrogating more than one SI, the OPD of each MZ sensing interferometer must differ by at least two times the coherence length of the source, $OPD1-OPD2 > 2Lc$. Increasing the difference between the OPDs of each SI reduces the crosstalk in the detected signal. Moreover, it enlarges the displacement range that can be measured without overlapping.

3. Experimental results

3.1. Displacement sensor at 290 km

The aim of the experiment was to evaluate the feasibility of monitoring an optical fiber interferometer at 290 km as a displacement sensor. For this purpose, we employed an ultra-long random distributed feedback laser in combination with FOLCI. Using the RDFB-FL structure previously presented, a sensor placed at a maximum distance of 250 km can be monitored by only injecting 3 W by one 1445 nm pump laser. However, in previous works it has been experimentally demonstrated that double pumping schemes are more efficient than pumping at a single wavelength [27–29]. Moreover, Raman assisted second-order amplification systems [30] can be employed to reach longer distances. As explained in Section 2, two pump lasers have been employed in the RDFB-FL scheme. An experimental study has been carried out to determine the optimum pump powers. Both values have been chosen so that the optical power reaching the sensing interferometer is maximized. The measured results show that the output power after 270 km present an upper limit, which is not surpassed despite increasing the injected pump powers. The optimum values are 3W in both pump lasers. In Fig. 4, the optical spectrum measured after 290 km (between the optical isolator and C1) is represented, showing a central wavelength set at 1555 nm and a peak power of -30.18 dBm.

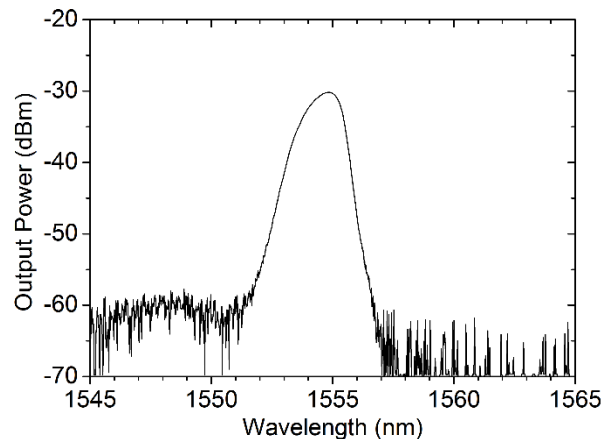


Fig. 4. Optical spectrum of the random DFB fiber laser measured after 290 km.

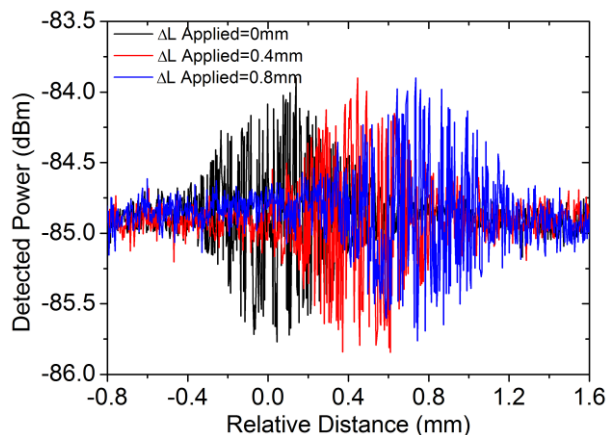


Fig. 5. Experimental traces detected at the output of the FOLCI scheme for three different sensor states.

To carry out this experiment, length variations have been induced and tracked in OPD1. The arm L2 of the SI has been fixed to a micro-positioner, with a resolution of 10 μm , to apply a displacement from 0 to 1 mm with 0.1 mm steps. Equivalently, the arm L2' in the LRI was attached to a separate micro-positioner (with a resolution of 20 nm) to perform the interrogation. In this manner, a displacement sweep was performed for 2.5 mm every 3.4 μm . After each complete sweep, it has been determined the central fringe position of the detected interferogram which represents the displacement of the SI.

The evolution of the interferogram detected is presented in Fig. 5. The measured signals for 0, 4 and 8 mm displacements are displayed, showing a clear shift of the central fringe. In order to ease the process of locating the central fringe, simple post-processing was applied by calculating the moving average of the absolute value of the data (Fig. 6). From the previous figures it can be inferred that the displacement of the central fringe position is clearly discernible and measurable.

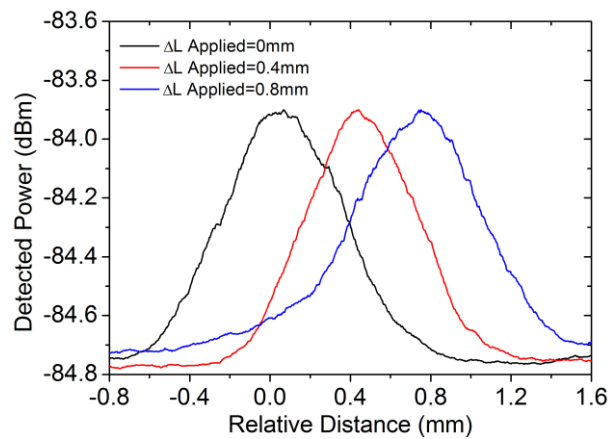


Fig. 6. Experimental traces detected at the output of the FOLCI scheme after post-processing.

The relative distance measurements that correspond to the peak of each trace are displayed in Fig. 7. In this graph, the displacement applied to the sensor versus the displacement measured shows a linear tendency with a slope of 1.03, $R^2 = 0.99$ and a resolution of 0.02mm. Some deviations in the experimental data are observed from the desired unity slope line. The intrinsic error of the micro-positioners and vibrations during the measuring process might be the cause.

Thus, a RDFB-FL in combination with a FOLCI scheme allowed to reach the longest distance in remote fiber optic sensing as far as the authors know, performing measurements at 290 km. This surpasses the 250 km distance limit already established in preceding remote monitoring publications.

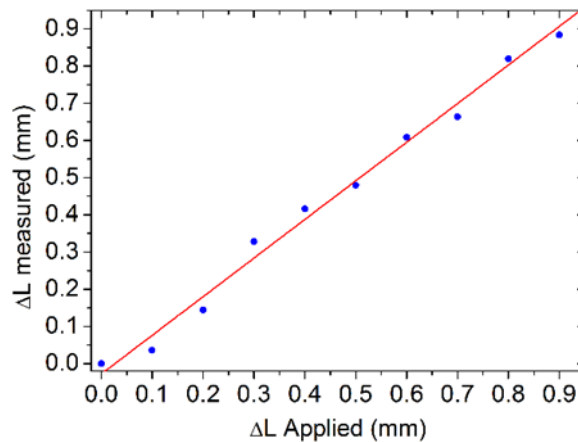


Fig. 7. Experimental displacement measurements for one sensor.

3.2. Coherence multiplexing of two displacement sensors at 270 km

In a second test, a set of measurements have been performed to validate the proposed system as a coherence multiplexing scheme. Using the setup depicted in Fig. 2, two MZI have been interrogated by the same displacement sweep at 270 km. Again this time, the pump powers of the laser source have been chosen to maximize the optical power arriving at the sensing interferometers. That is 3 W in both pump lasers. The optical spectrum measured after 270 km is represented in Fig. 8. The spectrum is centered at 1555 nm and shows a peak power of -25.21 dBm.

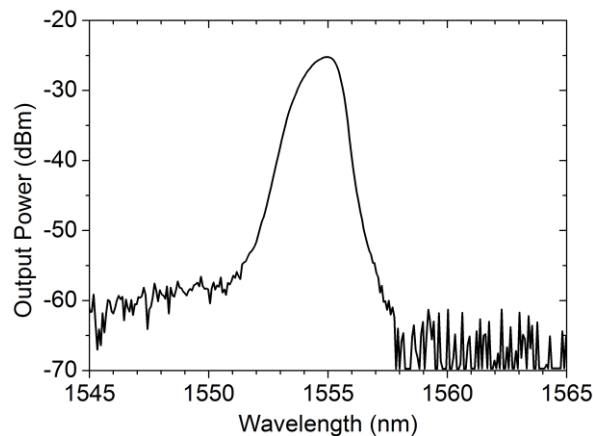


Fig. 8. Optical spectrum of the random DFB fiber laser measured after 270 km.

In order to evaluate the proper interrogation of the sensors, length variations were induced in SI1 using a micro-positioner with a resolution of $10\mu\text{m}$. In this manner, a displacement from 0 to 1 mm with 0.1 mm steps was applied to L2. The OPD in the SI2 was not modified during the experiment to prove the absence of crosstalk between the sensing interferometers. As in the first experiment, a displacement sweep was performed modifying the OPD of the LRI located at the header of the set-up (OPDr). Measurements were collected every $8.5\mu\text{m}$ using a micro-positioner with a resolution of 20 nm. Figure 9 shows the observed signals at the LRI output for 0 mm and 2 mm displacements. The same detected signals are presented in Fig. 10 after applying post-processing (as in 3.1). It can be seen in the figures that the displacement of the central fringe position of both SI1 and SI2 can be evidently determined.

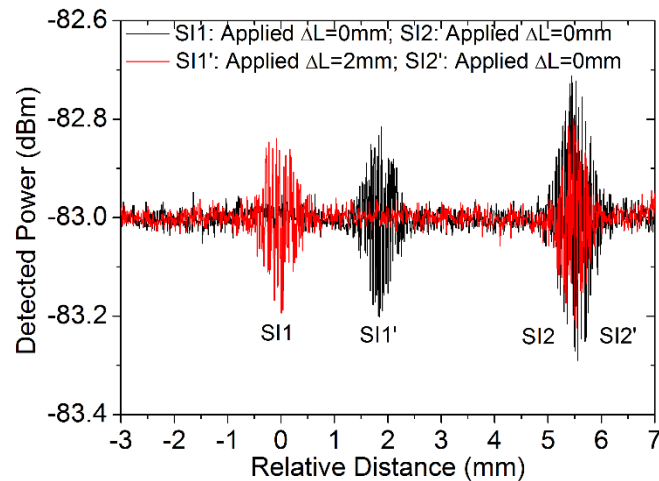


Fig. 9. Experimental traces detected at the output of the FOLCI scheme for three different sensor states.

It is also evidenced in the figure the lack of cross-talk since the interferogram of SI2 remains in a fixed position in all the displacement sweeps while SI1 shifts as we modify its OPD. It should be noted that the total displacement range is limited by the difference between the OPDs of the sensing interferometers. In this experiment, the band-gap between the OPDs of the sensors is 4 mm. As a result, the displacement range that can be measured without overlapping is 4 mm. However, if the OPD difference between sensing interferometers is adjusted, the displacement range can be increased depending on the application and its requirements.

Another aspect to be considered, common in every FOLCI system, is the total interrogation range, which is limited by the maximum displacement generated in the OPD of the receiving interferometer. In this experiment, simple elongation has been applied for the verification, but other solutions allow a wider range, such as the based on moving mirrors [15].

As discussed earlier in this work, the amplitude of the detected interferograms depends also on the instantaneous polarization state of the signals interfering. Accordingly, polarization has been controlled by means of a polarization controller in the LRI. A variation in the range of both SI2 and SI2' interferograms is appreciated due to these polarization changes. However, this issue could be addressed by including some polarization selective devices in the receiving interferometer, such as a polarization scrambler. Finally, the relationship between the displacement applied to the sensor and the measured one is represented in Fig. 11. As expected, the results show a linear tendency with a slope of 1.04, $R^2 = 0.98$ and a resolution of 0.02 mm.

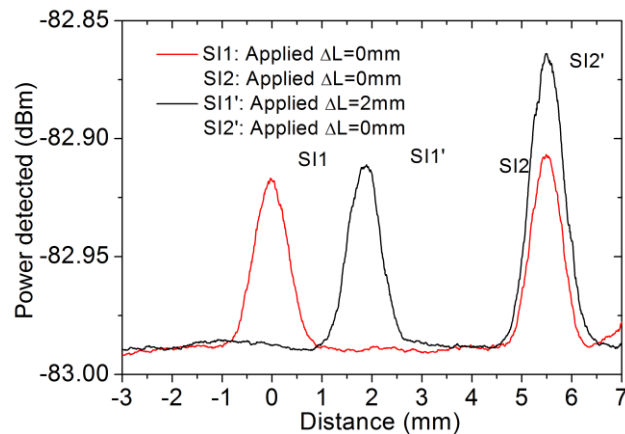


Fig. 10. Experimental traces detected at the output of the FOLCI scheme after post-processing.

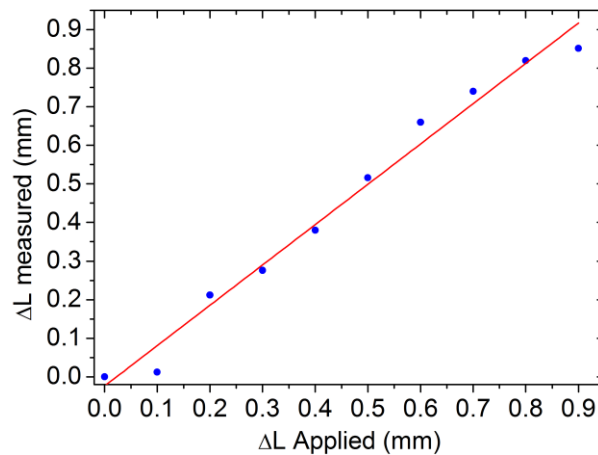


Fig. 11. Experimental displacement measurements for two sensors.

4. Conclusions

In this work, a proof of concept of a new application of RDFB-FL is presented. Its particular short coherence length has allowed its use as the light source in a remote FOLCI system for the first time. Furthermore, it has been demonstrated the feasibility of using this scheme for coherence-multiplexing. In order to perform the validation, a set of measurements has been carried out, exploiting the properties of this technique for remote sensing at long distances. In this manner, it has been reached the longest distance for a remote fiber optic sensing system, as far as the authors know.

An interferometric sensor has been monitored at a distance of 290 km and two interferometric sensors at 270 km, surpassing in both cases the 253 km distance milestone previously established in [7]. To achieve this, a double-pumped random DFB fiber laser has been combined with a low-coherence interferometry approach. This combination presents excellent properties for long distance applications. RDFB-FLs have been previously used in remote sensors monitoring due to their high output power, long cavities and high stability.

In previous proposals, the compatibility of TDM and WDM techniques with random DFB fiber lasers was demonstrated [10]. The experiments carried out and presented in this paper have also proved the feasibility of exploiting this type of lasers for coherence multiplexing of interferometric sensors. Taking into consideration power constrains, it has been estimated that a maximum of 8 sensors could be remotely multiplexed at 258 km and up to 16 at 248 km. New

hybrid approaches can be proposed, employing several multiplexing techniques simultaneously to increase the total number of sensors interrogated.

In the two experiments presented in this work, absolute displacements have been obtained for one and two sensors (coherence-multiplexed). The relationship between the displacement measured and the displacement applied show a linear trend with a slope of 1.03 and 1.04 respectively. Moreover, the results show the absence of crosstalk between the multiplexed sensors. These tests serve as a proof of concept, but the accuracy of the measurements could be enhanced by modifying the receiving interferometer setup (improve noise isolation or polarization control) and improving the accuracy of the mechanical sweep.

Funding

Spanish Comision Interministerial de Ciencia y Tecnología within project TEC2016-76021-C2-1-R as well as the FEDER funds, and by the Institute of Smart Cities by means of a postdoctoral fellowship.

References

1. A. G. Prasad, S. Asokan, and R. Tatavarti, "Detection of tsunami wave generation and propagation using fiber bragg grating sensors," *Sensors (Basel)* **2009**, 1278–1281 (2009).
2. N. Beverini, M. Calamai, D. Carbone, G. Carelli, N. Fotino, S. Gambino, R. Grassi, E. Maccioni, A. Messina, M. Morganti, and F. Sorrentino, "Strain sensors based on Fiber Bragg Gratings for volcano monitoring," *Fotonica AEIT Italian Conference on Photonics Technologies*, Turin, pp. 1–4 (2015).
3. L. Ren, H. Li, J. Zhou, D. S. Li, and L. Sun, "Health monitoring system for offshore platform with fiber Bragg grating sensors," *Opt. Eng.* **45**(8), 084401 (2006).
4. M. Fernandez-Vallejo and M. Lopez-Amo, "Optical fiber networks for remote fiber optic sensors," *Sensors (Basel)* **12**(4), 3929–3951 (2012).
5. T. Saitoh, K. Nakamura, Y. Takahashi, H. Iida, Y. Iki, and K. Miyagi, "Ultra-long-distance (230 km) FBG sensor system," in *19th International Conference on Optical Fibre Sensors (International Society for Optics and Photonics, 2008)* 7004, p. 70046C, (2008).
6. M. Fernandez-Vallejo, S. Rota-Rodrigo, and M. Lopez-Amo, "Remote (250 km) fiber Bragg grating multiplexing system," *Sensors (Basel)* **11**(9), 8711–8720 (2011).
7. M. Bravo, J. M. Baptista, J. L. Santos, M. Lopez-Amo, and O. Frazão, "Ultralong 250 km remote sensor system based on a fiber loop mirror interrogated by an optical time-domain reflectometer," *Opt. Lett.* **36**(20), 4059–4061 (2011).
8. A. D. Kersey, A. Dandridge, and A. B. Tveten, Overview of multiplexing techniques for interferometric fiber sensors," in *Fiber optic and laser sensors V (Vol. 838, pp. 184–194)*. International Society for Optics and Photonics, (1988).
9. J. S. S. M. S. Cusworth, "Multiplexing techniques for noninterferometric optical point-sensor networks: a review," *Fiber Integr. Opt.* **17**(1), 3–20 (1998).
10. D. Leandro, V. deMiguel Soto, R. A. Perez-Herrera, M. B. Acha, and M. López-Amo, "Random DFB fiber laser for remote (200 km) sensor monitoring using hybrid WDM/TDM," *J. Lightwave Technol.* **34**(19), 4430–4436 (2016).
11. M. J. L. Cahill, G. J. Pendock, and D. D. Sampson, "Hybrid coherence multiplexing/coarse wavelength-division multiplexing passive optical network for customer access," *IEEE Photonics Technol. Lett.* **9**(7), 1032–1034 (1997).
12. J. Brooks, R. Wentworth, R. Youngquist, M. O. S. H. E. Tur, B. Kim, and H. Shaw, "Coherence multiplexing of fiber-optic interferometric sensors," *J. Lightwave Technol.* **3**(5), 1062–1072 (1985).
13. D. M. Spirit, A. D. Ellis, and P. E. Barnsley, "Optical time division multiplexing: Systems and networks," *IEEE Commun. Mag.* **32**(12), 56–62 (1994).
14. B. Mukherjee, "WDM optical communication networks: progress and challenges," *IEEE J. Sel. Areas Comm.* **18**(10), 1810–1824 (2000).
15. D. Inaudi, S. Vurpillot, and S. L. Loret, "In-line coherence multiplexing of displacement sensors: a fiber optic extensometer," in *Smart Structures and Materials 1996: Smart Sensing, Processing, and Instrumentation (Vol. 2718, pp. 251–258)*. International Society for Optics and Photonics, (1996).
16. Z. G. Guan, D. Chen, and S. He, "Coherence multiplexing of distributed sensors based on pairs of fiber Bragg gratings of low reflectivity," *J. Lightwave Technol.* **25**(8), 2143–2148 (2007).
17. D. Inaudi, "Coherence multiplexing of in-line displacement and temperature sensors," *Opt. Eng.* **34**(7), 1912–1916 (1995).
18. M. E. Jones, J. L. Grace, J. A. Greene, T. A. Tran, V. Bhatia, K. A. Murphy, and R. O. Claus, "Multiplexed absolute strain measurements using extrinsic Fabry-Perot interferometers," in *Smart Structures and Materials 1995: Smart Sensing, Processing, and Instrumentation (Vol. 2444, pp. 267–276)*. International Society for Optics and Photonics, (1995).

19. S. A. Al-Chalabi, B. Culshaw, and D. E. N. Davies, "Partially coherent sources in interferometric sensors," in First International Conference on Optical Fibre Sensors (pp. 26–28), (1983).
20. Y. J. Rao and D. A. Jackson, "Recent progress in fibre optic low-coherence interferometry," *Meas. Sci. Technol.* **7**(7), 981–999 (1996).
21. H. S. Choi, H. F. Taylor, and C. E. Lee, "High-performance fiber-optic temperature sensor using low-coherence interferometry," *Opt. Lett.* **22**(23), 1814–1816 (1997).
22. K. Totsu, Y. Haga, and M. Esashi, "Ultra-miniature fiber-optic pressure sensor using white light interferometry," *J. Micromech. Microeng.* **15**(1), 71–75 (2005).
23. C. Belleville and G. Duplain, "White-light interferometric multimode fiber-optic strain sensor," *Opt. Lett.* **18**(1), 78–80 (1993).
24. M. Jedrzejewska-Szczerska, M. Gnyba, and B. B. Kosmowski, "Low-coherence fibre-optic interferometric sensors," *Acta Phys. Pol. A* **120**(4), 621–624 (2011).
25. S. K. Turitsyn, S. A. Babin, A. E. El-Taher, P. Harper, D. V. Churkin, S. I. Kablukov, J. D. Ania-Castañón, V. Karalekas, and E. V. Podivilov, "Random distributed feedback fibre laser," *Nat. Photonics* **4**(4), 231–235 (2010).
26. Y. J. Rao and W. L. Zhang, "Recent progress in random fiber lasers," In *Optical Communications and Networks (ICOCN)*, 2013 12th International Conference on (pp. 1–4). IEEE (2013).
27. X. H. Jia, Y. J. Rao, Z. N. Wang, W. L. Zhang, Y. Jiang, J. M. Zhu, and Z. X. Yang, "Towards fully distributed amplification and high-performance long-range distributed sensing based on random fiber laser." In *OFS2012 22nd International Conference on Optical Fiber Sensors (Vol. 8421, p. 842127)*. International Society for Optics and Photonics, (2012).
28. A. E. El-Taher, M. Alcon-Camas, S. A. Babin, P. Harper, J. D. Ania-Castañón, and S. K. Turitsyn, "Dual-wavelength, ultralong Raman laser with Rayleigh-scattering feedback," *Opt. Lett.* **35**(7), 1100–1102 (2010).
29. J. Ania-Castañón, "Quasi-lossless transmission using second-order Raman amplification and fibre Bragg gratings," *Opt. Express* **12**(19), 4372–4377 (2004).
30. S. Martin-Lopez, M. Alcon-Camas, F. Rodriguez, P. Corredera, J. D. Ania-Castañón, L. Thévenaz, and M. Gonzalez-Herraez, "Brillouin optical time-domain analysis assisted by second-order Raman amplification," *Opt. Express* **18**(18), 18769–18778 (2010).